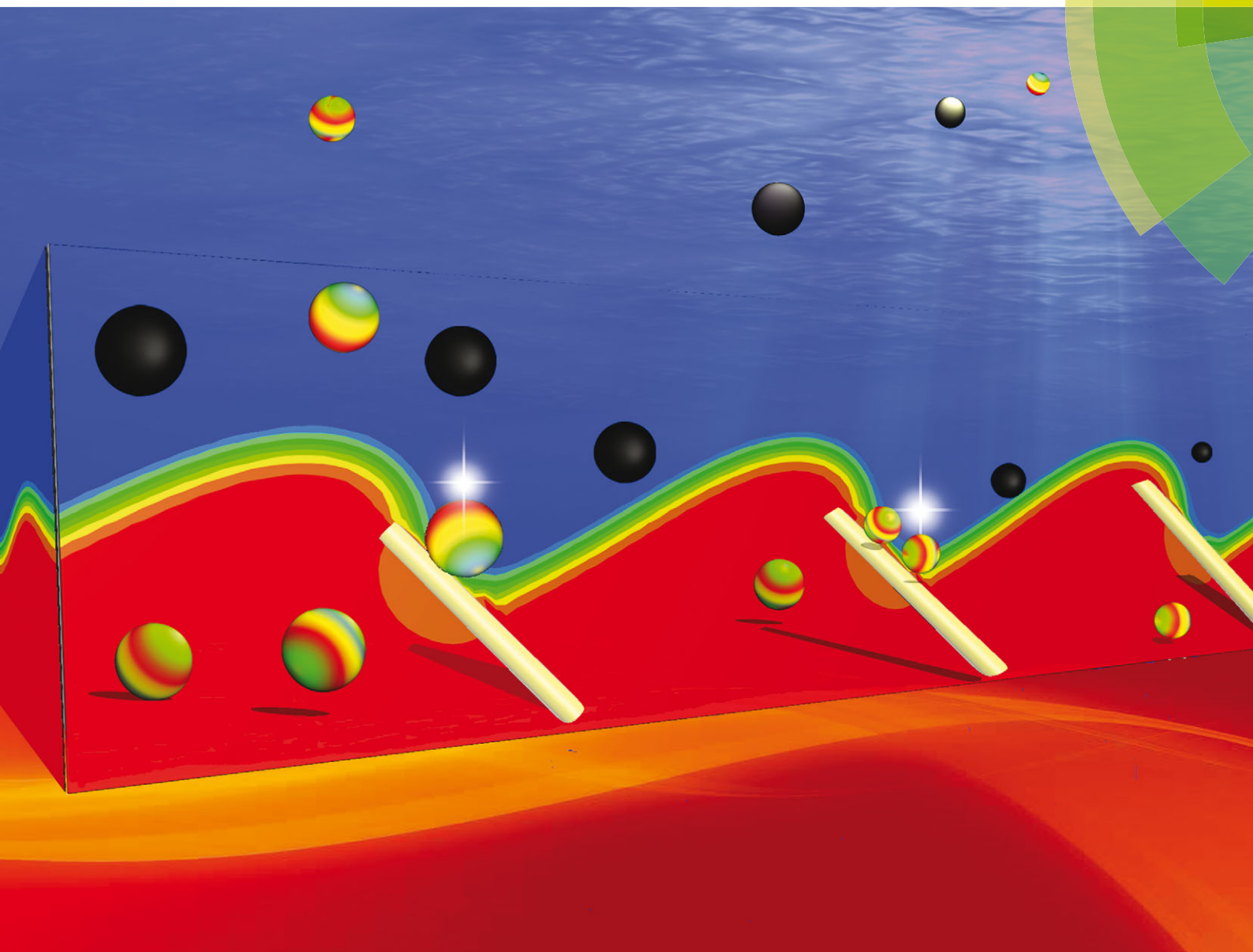


# Soft Matter

www.softmatter.org



ISSN 1744-683X



ROYAL SOCIETY  
OF CHEMISTRY

PAPER

Anna C. Balazs *et al.*  
Computational modeling of oscillating fins that “catch and release”  
targeted nanoparticles in bilayer flows

**175** YEARS



Cite this: *Soft Matter*, 2016, 12, 1374

# Computational modeling of oscillating fins that “catch and release” targeted nanoparticles in bilayer flows†

Ya Liu,<sup>a</sup> Amitabh Bhattacharya,<sup>b</sup> Olga Kuksenok,<sup>c</sup> Ximin He,<sup>de</sup> Michael Aizenberg,<sup>f</sup> Joanna Aizenberg<sup>fg</sup> and Anna C. Balazs<sup>\*a</sup>

A number of physiological processes in living organisms involve the selective “catch and release” of biomolecules. Inspired by these biological processes, we use computational modeling to design synthetic systems that can controllably catch, transport, and release specific molecules within the surrounding solution, and, thus, could be harnessed for effective separation processes within microfluidic devices. Our system consists of an array of oscillating, microscopic fins that are anchored onto the floor of a microchannel and immersed in a flowing bilayer fluid. The oscillations drive the fins to repeatedly extend into the upper fluid and then tilt into the lower stream. The fins exhibit a specified wetting interaction with the fluids and specific adhesive interactions with nanoparticles in the solution. With this setup, we determine conditions where the oscillating fins can selectively bind, and thus, “catch” target nanoparticles within the upper fluid stream and then release these particles into the lower stream. We isolate the effects of varying the wetting interaction and the fins’ oscillation modes on the effective extraction of target species from the upper stream. Our findings provide fundamental insights into the system’s complex dynamics and yield guidelines for fabricating devices for the detection and separation of target molecules from complex fluids.

Received 8th November 2015,  
Accepted 7th December 2015

DOI: 10.1039/c5sm02752g

[www.rsc.org/softmatter](http://www.rsc.org/softmatter)

## 1. Introduction

A number of vital technological processes involve the selective binding, transport and release of targeted species. For example, such “catch and release” events are crucial for the detection and separation of biomolecules,<sup>1–12</sup> as well as the filtration and purification of particulate-filled fluids. It remains, however, a challenge to design effective small-scale devices that are portable and thus, could be used at the point of care. In this

context, microfluidics provides an optimal platform for such systems. Ideally, these systems should encompass separate inlet and outlet fluid streams so that the multiple components could be introduced in one fluid and the targeted species could be collected in another, separate fluid. The system also needs a smart “hook” to selectively catch the targeted species. Finally, models that could provide physical insight into the complex dynamic, multi-stage phenomena occurring in these systems would be highly useful for optimizing the performance of the device.

In recent studies,<sup>13,14</sup> we devised a hybrid, multi-component system, where microscopic fins were partially embedded in a stimuli-responsive gel. This composite was encased in a microfluidic chamber where a pressure driven, two-phase fluid washed over the entire system. The rhythmic motion of the gel layer caused the embedded fins to move back and forth between the top and bottom layers of the two fluid streams. The fins acted as the smart hooks;<sup>14</sup> namely, their movements were harnessed to selectively bind and transport dissolved species in the top layer and bring these species into the lower layer, where they were collected and removed.<sup>14</sup> In this manner, the system provided an effective device for performing “catch and release” functions.

In the latter studies,<sup>14</sup> we developed a computational model to simulate the salient features of the experiments, tuning our simulation parameters to capture the overall behavior of the system. Using this model, we then predicted how to modify the

<sup>a</sup> Department of Chemical and Petroleum Engineering, University of Pittsburgh, Pittsburgh, PA, USA. E-mail: [balazs@pitt.edu](mailto:balazs@pitt.edu)

<sup>b</sup> Department of Mechanical Engineering, Indian Institute of Technology Bombay, Powai, Maharashtra, India

<sup>c</sup> Department of Materials Science and Engineering, Clemson University, Clemson, SC, USA

<sup>d</sup> Molecular Design and Biomimetics Center, Biodesign Institute, Arizona State University, Tempe, AZ, USA

<sup>e</sup> Materials Science and Engineering, School for Engineering of Matter, Transport and Energy, Arizona State University, Tempe, AZ, USA

<sup>f</sup> Wyss Institute for Biologically Inspired Engineering, Harvard University, Cambridge, MA, USA

<sup>g</sup> Department of Chemistry and Chemical Biology, Harvard University, Cambridge, MA, USA

<sup>h</sup> John A. Paulson School of Engineering and Applied Sciences, Harvard University, Cambridge, MA, USA

† Electronic supplementary information (ESI) available. See DOI: 10.1039/c5sm02752g

experimental setup to improve the efficiency of the device and found good agreement between our predictions and the experimental results. In modeling the system, we assumed that the interface between the two fluids remained flat, as was the case in the experiments,<sup>14</sup> due to specific features of the setup. Here, we use the latter studies as a springboard to formulate a new computational approach that allows us to consider more general scenarios where wetting interactions along mobile, microscopic solids affect the evolution of the fluids and the motion of nanoscopic particulates dispersed within these fluids. In this manner, we can focus on the complex dynamic interactions occurring at the fin–fluid and fluid–fluid interfaces, and thereby, gain a greater understanding of factors that can affect the selective trapping and release of the particulates.

Specifically, we now take into account the fact that fins can cause perturbations to the fluid–fluid interface as they oscillate between the layers. Moreover, we specify the wetting interactions between the fins and fluids. Hence, the system can encompass complex hydrodynamic interactions, which would also affect the dispersion of particulates in the system. To the best of our knowledge, this is the first computational model to describe the dynamic behavior of systems containing all the following: mobile fins with spatially-dependent wetting properties, binary fluids with evolving interfaces, and mobile, interactive nanoparticles. By accounting for this range of phenomena, our approach can be adapted to model the mixing and processing of a range of multi-component, multi-scale systems, and thus, enhance our understanding of cooperative interactions that can occur during the structural evolution of the complex fluids.

As noted above, the gel in the “catch and release” device provides the “muscle” that drives the oscillatory motion of the embedded fins. Namely, this gel can be made to repeatedly expand and contract by, for instance, altering the temperature<sup>13</sup> or the pH<sup>14</sup> of the fluid that washes over the system. As we showed in previous studies,<sup>13,14</sup> the contraction of the gel drives the fins to dip away from the top fluid and extend into the lower layer. Conversely, the expansion of the gel drives the fins to move from the lower layer and extend into the upper fluid. (Alternatively, fins could be actuated to undergo periodic oscillatory motion by applying external magnetic fields.<sup>15–17</sup>)

Fig. 1 shows snapshots of the fins and the two immiscible liquids forming the bilayer fluid. We model immiscible fluids confined between two walls in order to simulate experiments that encompassed organic and aqueous phases<sup>13</sup> or two aqueous phases that were maintained as separate streams in microfluidic devices through the uses of distinct inlets and imposed flow.<sup>14</sup> An imposed pressure gradient causes the fluid to flow from left to right within the channel. The stimuli-responsive gel (not shown) is assumed to form the underlying substrate. In the studies described here, we introduce a binary particle mixture in the upper fluid stream. This mixture includes adhesive and non-adhesive particles; the adhesive species are the targeted particles in these studies. Importantly, the adhesive particles exhibit a preferential binding interaction with the portions of the fins that extend into the upper fluid. It is through this

favorable binding interaction that the fins can trap the targeted particles. Experimentally, these favorable interactions could be achieved by coating the fins with chemical entities carrying recognition motifs, such as aptamers that bind to specific target molecules.<sup>14</sup> As the fins are driven to move into the lower solution, the bound target particles are brought into contact with this fluid. Once localized in this bottom layer, the fin–particle bond is broken and the particle is thereby released into this lower stream. The latter action mimics the breakage of the aptamer–target bond due, for example, to the denaturation of the aptamers in the lower fluid (which can have a different pH from the upper fluid and thus, promote this denaturation).<sup>14</sup> Once the targeted particles are sequestered and released into the lower stream, they can be collected from this fluid. Notably, the aptamer denaturation is reversible,<sup>18</sup> and hence, when the aptamer-coated fin is driven into the upper stream by the underlying gel, the fin sites in this upper fluid are once again able to trap new target particles within this fluid.

The simulations described below are aimed at gaining insight into factors that affect the efficiency and selectivity of this catch and release device and thus, provide design rules for optimizing the performance of the system. On a more general level, the findings also reveal the intricate dynamic behavior that arises from the interplay among the mobile particles, a temporally evolving interface, the oscillating fins, the wetting interactions between the fins and fluids, and the dynamically changing binding interactions. We emphasize that such studies also offer valuable insight into the properties of chemically reactive mixtures that are subjected to imposed flows and modes of mixing, as well as enhance our understanding of complex hydrodynamic interactions occurring in multi-component mixtures in confined geometries.

By integrating features of different computational models,<sup>19–32</sup> we formulate a new hybrid approach to simulate the range of interactions encompassed in this multi-component, dynamic system. In particular, we couple the lattice Boltzmann model (LBM)<sup>26,27</sup> for binary fluids with a stochastic differential equation for the motion of the nanoparticles and introduce fins that are described as rigid rods anchored to a substrate. We also incorporate the wetting interactions between the fins and the fluids, as well as the adhesive interactions between the fins and the particles in the solution. The approach is detailed in the Methods section, where we also relate our simulation parameters to physical values. Below, we describe the effects of varying the wetting interactions between the oscillating fins and the fluid, the number of particles in the system, and the fins’ mode of oscillation.

## II. Methodology

### A. Description of model

Our system encompasses an immiscible 50:50 AB binary mixture that is driven by an imposed gradient pressure to flow through a microchannel. This incompressible AB binary mixture is characterized by the continuous order parameter,

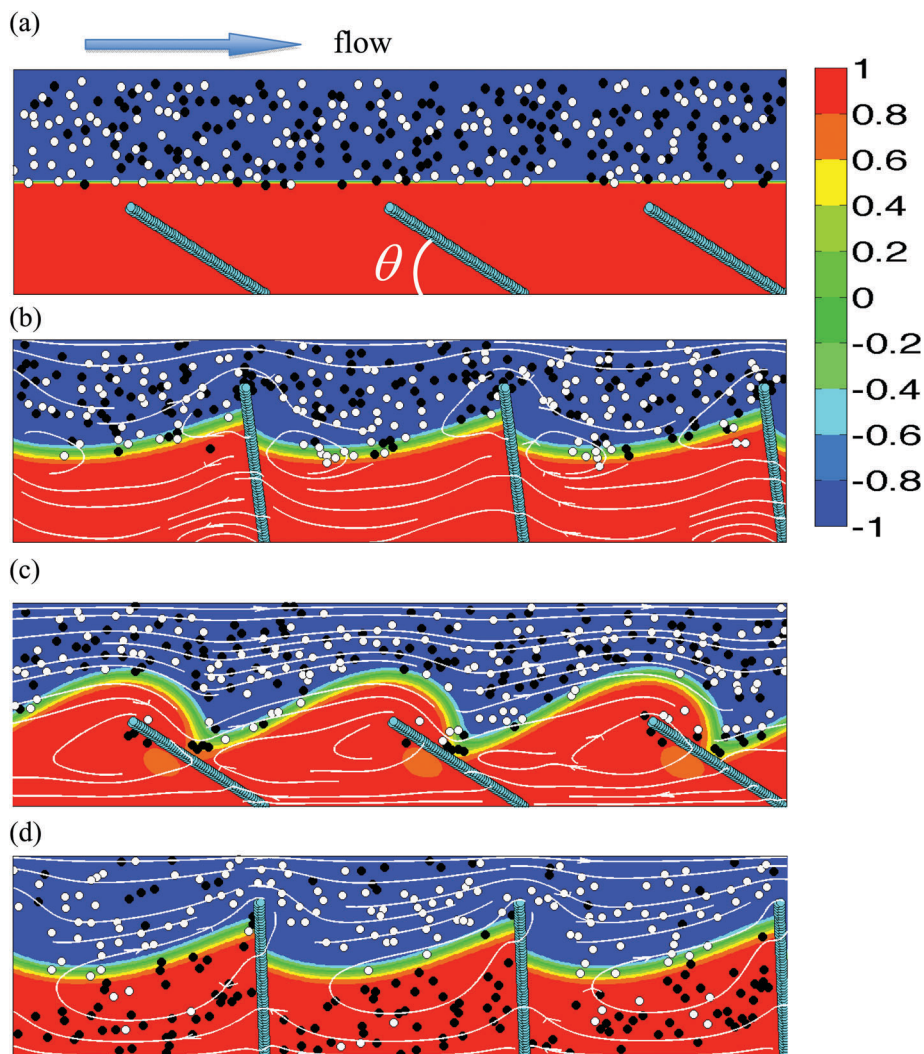


**Fig. 1** Snapshots of the system, illustrating mechanism of oscillating fins “catching and releasing” particles within a binary blend. (a) The initial morphology of the system with two types of particles, adhesive (in black) and nonadhesive (in white), randomly distributed in upper stream. The blend is represented by the value of order parameter  $\phi(\mathbf{r})$  as illustrated by the color bar. The oscillating angle  $\theta$  varies from  $\pi/6$  to  $\pi/2$ . (b) Fins catch adhesive particles in the upper stream, where the fluid streamlines are shown in white at  $t = 3 \times 10^4$ . (c) Attached adhesive particles are released from fins when immersed at  $t = 3.2 \times 10^5$ . (d) Late-time morphology of the system at  $t = 5 \times 10^6$ .

$\phi$ , defined as the difference between the local mass density of the A and B components:  $\phi = (\rho_A - \rho_B)/\rho$ , where  $\rho = \rho_A + \rho_B$  is the total mass density of the fluid.<sup>19</sup> The values  $\phi = 1$  and  $-1$  correspond, respectively, to the A-rich (lower red) and B-rich (upper blue) phase (see Fig. 1(a)).

An array of fins is submerged into this binary fluid stream and is anchored to the floor of the microchannel. The fins undergo externally driven oscillations. During the oscillations, the fins reach into the upper fluid (B-rich phase) when they are upright and are entirely immersed within the lower stream (A-rich phase) when they are tilted. At the onset of the simulations, we introduce a binary mixture of mobile nanoparticles into the upper fluid: the black nanoparticles can adhere to the fins, while the white particles are non-adhesive (Fig. 1(a)). The portion of the fins that extend into the upper B stream can bind the neighboring adhesive particles.

The free energy functional that describes the nanoparticle-filled AB binary mixture can be written as:<sup>19</sup>

$$F = \int \left[ \psi_b(\phi, \rho) + \frac{\kappa}{2} |\nabla \phi|^2 \right] d\mathbf{r} + \int \psi_s(\phi_s) ds \quad (1)$$

where  $\psi_b(\phi, \rho)$  is the Landau-Ginzburg free energy for the binary fluid and is given by:

$$\psi_b(\phi, \rho) = \frac{1}{3} \rho \ln \rho - \frac{a}{2} \phi^2 + \frac{b}{4} \phi^4. \quad (2)$$

The second term in the first integral characterizes the energy penalty for creating spatial variations of the order parameter and is thus related to the interfacial tension  $\sigma = \sqrt{8\kappa a^3/9b^2}$ . When the parameters  $a$ ,  $b$ , and  $\kappa$  are positive constants, the binary mixture spontaneously phase-separates into A-rich and B-rich domains with the interfacial width equal to  $\xi = 5\sqrt{\kappa/2a}$ .

The equilibrium value of the order parameters is  $\phi = \sqrt{a/b}$  and  $\phi = -\sqrt{a/b}$  for A-rich and B-rich phases, respectively.

The second integral in eqn (1) represents the wetting interactions at the fluid–solid boundaries that depend on the distribution of the order parameters on the interface  $\phi_s$ :  $\psi_s(\phi_s) = -h\phi_s$ ,<sup>20</sup> where  $h$  is a tunable parameter that characterizes the strength of the wetting interaction. The value of  $h$  is related to the static contact angle  $\theta_{st}$ :<sup>21,22</sup>

$$h = \sqrt{2\kappa b} \text{sgn}(\pi/2 - \theta_{st}) \sqrt{\cos(\alpha/3)(1 - \cos(\alpha/3))}, \quad (3)$$

where  $\text{sgn}(x)$  is the sign function and  $\alpha = \arccos(\sin^2\theta_{st})$ . In our system, we specify the wetting interactions between the following: (1) the binary fluids and the top and bottom walls of the microchannel, and (2) the binary fluids and the fins. By minimizing the free energy functional (eqn (1)) with respect to the order parameter at the boundary between the fins and the binary mixture, we obtain the following boundary condition:<sup>23</sup>

$$\mathbf{n} \cdot \nabla \phi = -h/\kappa, \quad (4)$$

where  $\mathbf{n}$  is the unit vector normal to the interface.

The temporal evolution of the order parameter is governed by the following convection-diffusion equation:

$$\frac{\partial \phi}{\partial t} + \nabla(\phi \mathbf{u}) = M \nabla^2 \mu \quad (5)$$

Here,  $M$  is the mobility of the order parameter,  $\mu$  is the chemical potential related to the free energy functional:  $\mu = \delta F/\delta \phi$  and  $\mathbf{u}(\mathbf{r}, t)$  is the fluid velocity. The dynamics of nanoparticle-filled fluid is described by the Navier-Stokes equation:

$$\frac{\partial}{\partial t}(\rho \mathbf{u}) + \nabla(\rho \mathbf{u} \mathbf{u}) = -\nabla \cdot \mathbf{P} + \eta \nabla^2 \mathbf{u} + \mathbf{G}^{\text{drag}}, \quad (6)$$

where  $\mathbf{P}$  is the pressure tensor and  $\eta$  is the viscosity of the fluid. We impose no-slip boundary conditions on the moving fins and the top and bottom walls and hence, in the absence of the fins, the flow exhibits a parabolic profile.

The last term,  $\mathbf{G}^{\text{drag}}$ , arises from viscous drag acting on the nanoparticles:<sup>20</sup>

$$\mathbf{G}^{\text{drag}}(\mathbf{r}) = - \sum_i \delta(\mathbf{r} - \mathbf{r}_i) \mathbf{F}^{\text{drag},i} \quad (7)$$

Here,  $\mathbf{F}^{\text{drag},i} = -\zeta[\dot{\mathbf{r}}_i(t) - \mathbf{u}(\mathbf{r}_i, t)]$  is the frictional drag force on the  $i$ th nanoparticle with the friction coefficient being  $\zeta = 6\pi\eta R_p$ . The radius of the nanoparticles is sufficiently small ( $R_p = 0.096$ ) that we model these species as tracer particles. The dynamic behavior of these nanoparticles is governed by the following stochastic differential equation:

$$d\mathbf{r}_i(t) = \mathbf{u}(\mathbf{r}_i, t) dt + \sqrt{2D_p} d\mathbf{W}_i(t) + \frac{dt}{\zeta} [\mathbf{F}_i^c(t) + \mathbf{F}_i^a(t)] \quad (8)$$

The first term on the right-hand-side accounts for the drift velocity due to the fluid motion. The second term represents the random force acting on the  $i$ th particles and satisfies the fluctuation-dissipation relation:  $\langle \mathbf{W}_i(t) \cdot \mathbf{W}_j(t') \rangle = 2k_b \text{TD}_p \delta_{ij} \delta(t - t')$ . The term  $\mathbf{F}_i^c(t)$  in eqn (8) represents the nanoparticle–nanoparticle and nanoparticle–fin excluded volume interactions. This interaction

is modeled by the repulsive part of the Morse potential, which has the following form:<sup>24</sup>

$$\psi_m(r) = \varepsilon(1 - \exp[-\lambda(r - r_c)])^2, \quad (9)$$

where the values of  $\varepsilon$  and  $\lambda$  define the strength and range of the potential, and  $r_c$  is the relevant equilibrium separation. The parameter  $\psi_m(r)$  is repulsive if  $r < r_c$  and attractive if  $r > r_c$ ; to prevent the overlap between the particles, and between the particles and fins, the potential for the excluded volume interaction is applied when  $r < r_c$ . The repulsive force is

derived from the relation  $\mathbf{F}_i^c(t) = -\nabla_i \sum_{j \neq i}^N \psi_m(|r_i - r_j|)$ , where  $\mathbf{r}_i$

represents the center of mass of the nanoparticles or a site on the fins, and  $\nabla_i = [\partial/\partial r_{i,x} \mathbf{i} + \partial/\partial r_{i,y} \mathbf{j}]$ . The force  $\mathbf{F}_i^a(t)$  in eqn (8) accounts for the attractive interaction between the fins and adhesive particles in the upper stream.

Driven by an externally applied force, the fins oscillate between  $\theta_{\min}$  and  $\theta_{\max}$ , the respective minimum and maximum angles formed between the fins and floor of the microchannel. Given that the period of oscillations is  $T$ , the temporal variation in the angle between the fins and floor is given by:

$$\theta(t) = \frac{1}{2}(\theta_{\max} + \theta_{\min}) - \frac{1}{2}(\theta_{\max} - \theta_{\min}) \cos \frac{2\pi t}{T} \quad (10)$$

The corresponding angular velocity of the fins is given by  $\omega(t) = \frac{\pi}{T}(\theta_{\max} - \theta_{\min}) \sin \frac{2\pi t}{T}$ ; the value of  $\omega$  is zero when  $\theta(t)$  reaches  $\theta_{\min}$  or  $\theta_{\max}$ . Such oscillations could be realized experimentally by applying an oscillatory magnetic field to magneto-responsive fins. Alternatively, the fins could be embedded into hydrogels that contract and expand due to changes in pH or temperature;<sup>13</sup> hence, periodic changes in the latter stimuli can be utilized to drive the oscillation of the fins.

Recall that our aim is to determine the extent to which the fins can selectively bind target species that are dispersed in the upper solution. Here, the target species are modeled as the adhesive particles and our goal is to determine the fraction of these adhesive particles that the fins can “catch” relative to the total particles in the system. Specifically, the portion of the fin that extends into the upper fluid can selectively bind the adhesive nanoparticles; the non-adhesive particles do not bind to the fins. To model this selective attraction, we introduce a bond-like interaction between the adhesive nanoparticles and the sites on the fins located in upper stream. In particular, an attractive Morse potential with the same form as eqn (9) and given by  $\psi_a = \varepsilon(1 - \exp[-\lambda(|\mathbf{r}_p - \mathbf{r}_f| - r_c)])^2$  is applied when  $r_c \leq |\mathbf{r}_p - \mathbf{r}_f| < r_b$ , where  $\mathbf{r}_p$  and  $\mathbf{r}_f$  are the respective positions of the centers of the adhesive particles and the fin sites.<sup>25</sup> Consequently, the bond that forms has an effective length of  $r_b = r_c + \ln 2/\lambda$ .<sup>25</sup> If the separation between adhesive nanoparticles and the fins is greater than the bond length, *i.e.*, when  $|\mathbf{r}_p - \mathbf{r}_f| \geq r_b$ , the above potential is no longer applied; when  $|\mathbf{r}_p - \mathbf{r}_f| < r_c$ , the excluded volume interaction described by eqn (9) dominates. Importantly, an adhesive site on a fin can form only a single bond with the adhesive nanoparticle. Hence, the number of the adhesive sites effectively limits

the maximum number of nanoparticles that can potentially be collected by the fins. In the simulations below, we set the parameters to the following values:  $\lambda = 0.8$ ,  $\varepsilon = 1.5$  and  $r_c = 1.2$ .

Eqn (4) and (6) are resolved by using the Lattice Boltzmann method (LBM),<sup>26,27</sup> which has proven to be an efficient method for modeling the complex fluid dynamics in systems that encompass multiple length scales. Since the boundary condition in eqn (4) is applied on the oscillatory fins, we therefore use a computational method that combines the bounce-back scheme and interpolations of the order parameter on the moving boundary.<sup>28–30</sup> Consequently the conservation of the order parameter and linear momentum of the binary fluids is preserved.

## B. Simulation setup and model parameters

In our simulations, we solve the governing equations on a two-dimensional channel, with periodic boundary conditions applied on the horizontal direction and bounce-back conditions on the top and bottom of the channel. The channel size is  $40 \times 150$  in dimensionless units. While we carry out the simulations in 2D, the model does capture fundamental features of 3D experimental systems when, for example, the fins are broad in the third dimension (*i.e.*, into the page). The static contact angle between the respective fluid and the walls of the channel is set to  $\theta_{st}^w = \pi/3$ . The fins are 30 LB lattice spacing units in length and the oscillation period  $T = 1.5 \times 10^5$ . The applied pressure gradient is fixed at  $P_x = -5 \times 10^{-5}$ . The values of model parameters in eqn (1) and (2) are set to  $a = b = 0.01$  and  $\kappa = 0.02$ . Hence, the width of interface is  $\zeta \approx 5$ , and the interfacial tension is  $\sigma \approx 0.013$ . The fluid density is set to  $\rho = 1$ , the dynamic viscosity of both fluids  $\eta = 1/6$ , and the mobility of the order parameters  $M = 1$ .

Our simulation parameters can be related to their physical values by using  $L_0 = \eta^2/(\rho\sigma)$ ,  $T_0 = \eta^3/(\rho\sigma^2)$ , where  $L_0, T_0$  are the characteristic length scale and time scale, respectively.<sup>31,32</sup> At room temperature, using  $\rho = 10^{-3} \text{ kg m}^{-3}$ ,  $\eta = 1.0 \times 10^{-3} \text{ Ns m}^{-2}$  and  $\sigma = 6.0 \times 10^{-4} \text{ N m}^{-1}$ , we obtain the physical values of the dimensionless unit of the lattice spacing and time scale as:  $L_0 \approx 0.8 \text{ }\mu\text{m}$  and  $T_0 \approx 10^{-7} \text{ s}$ . Using these estimates and given that  $R_p = 0.096$ , the size of nanoparticles are specified as 77 nm. Similarly, we obtain the length of fins as  $L_{fin} = 24 \text{ }\mu\text{m}$ , the height of the channel as  $W = 32 \text{ }\mu\text{m}$ , and the oscillation frequency as  $f = 66 \text{ Hz}$ . The fluid velocity measured directly from the simulations does not exceed  $3 \times 10^{-3}$ , which corresponds to  $2.4 \times 10^{-2} \text{ m s}^{-1}$ . Given the dimensionless diffusivity of particles  $D_p = 10^{-5}$ , one obtains the value of the diffusion constant to be  $6.4 \times 10^{11} \text{ m}^2 \text{ s}^{-1}$ .

With the applied pressure gradient fixed at  $P_x = -5 \times 10^{-5}$ , the fluid velocity measured directly from the simulations does not exceed  $3 \times 10^{-3}$  dimensionless units. This, in turn, corresponds to  $2.4 \times 10^{-2} \text{ m s}^{-1}$ , which is an experimentally feasible value within microfluidic devices.

## III. Results and discussion

At the onset of the simulations, the adhesive (black) and non-adhesive (white) nanoparticles are randomly distributed within

the upper fluid stream; initially, there are no particles within the lower stream, as shown in Fig. 1(a). The imposed pressure gradient drives the fluid to flow from left to right within the channel; note that periodic boundary conditions are applied along the lateral direction of the two-dimensional simulation box. We first consider a total of  $N = 300$  nanoparticles, which are equally divided into  $N_a = 150$  adhesive and  $N_n = 150$  non-adhesive species. The three equally-spaced fins on the bottom of the channel are initially totally immersed in the lower stream with  $\theta = \theta_{min} = \pi/6$  (Fig. 1(a)). The maximal angle formed between the fins and bottom wall is  $\theta_{max} = \pi/2$ . The preferential wetting interactions between the fins and the fluids are controlled by setting the static contact angle  $\theta_{fin} = \pi/2.5$  through eqn (4) and (5). To verify that the contact angle between the A/B interface and the fins in the simulations is equal to the specified value of  $\pi/2.5$ , we performed independent computer runs and found that the error between the value in the simulations and the specified value of  $\theta_{fin}$  was less than 3%.

Only the fin sites that extend into the upper stream are “activated”, and thus, can “catch” (bind) the adhesive nanoparticles. The binding interaction involves the formation of bonds between the activated fin sites and the particles. The oscillating fins, however, are driven to move back and forth between the two fluid streams. Thus, when these sites are brought into the lower fluid, the bonds are broken instantaneously and the respective fin sites become deactivated, rendering them non-adhesive to both types of nanoparticles.

The transport of nanoparticles within this system can occur through three distinct processes, which we will label (1)–(3). Process (1) involves the selective capture of the targeted adhesive nanoparticles through their attraction to the fin in the upper stream, their transport into the lower stream and the subsequent breakage of the bonds. Process (2) involves the motion of nanoparticles along the streamlines generated by the combination of the external pressure gradient and the fins’ oscillatory motion; depending on the resulting flow profiles, these streamlines could bring both types of nanoparticles (adhesive and non-adhesive) into the lower fluid or pump them back into the upper fluid. Process (3) involves the diffusion of nanoparticles between the upper and lower fluid layers.

Process (1) depends not only on the range and strength of the adhesive interaction, but also on the number density of the nanoparticles and availability of the adhesive fin sites in the upper fluid stream. As illustrated in Fig. 1(b), fin sites within the upper stream can successfully catch the adhesive particles. As the fins move downward, the bound adhesive particles follow the motion of fins and are delivered into the lower stream; thereafter, the bonds are broken and those adhesive particles are released as illustrated in Fig. 1(c).

Due to process (2), however, a small number of non-adhesive particles are also delivered in the lower stream (see white particles in Fig. 1(c)). As noted above, the fluid convection in our system is induced by the combination of the fins’ motion and the imposed pressure gradient. The flow close to the fins, however, is determined mainly by the motion of the fins. Therefore, if nanoparticles of either type happen to lie close to the fins, they are easily driven into the lower stream as the

fins move downward and are pumped back into the upper stream as fins move upward. In other words, process (2) is non-selective and could lead to the delivery of non-adhesive particles into the lower stream. (In general, process (2) is controlled by the channel geometry, the imposed flow, the fins' arrangement and mode of oscillation.)

As demonstrated below, by tuning the interplay between processes (1) and (2) and with the proper choice of parameters, one can obtain conditions where the majority of the adhesive particles are brought into the lower stream and the majority of non-adhesive particles are localized in the upper stream (as shown at  $t = 5 \times 10^6$  in Fig. 1(d)). We note that the diffusion coefficient of the nanoparticles ( $D_p \approx 6.4 \times 10^{-11} \text{ m}^2 \text{ s}^{-1}$ ) is sufficiently small compared to the motion of the fluids from the imposed flow and the fins' oscillation so that the contribution from process (3) is significantly smaller than the contributions from processes (1) and (2).

An experimentally feasible means of manipulating the physical properties of the interface, and consequently tuning the interplay between processes (1) and (2), is to modify the value of the static wetting angle  $\theta_{\text{fin}}$  (see Fig. 2). Two distinct differences are observed if we compare the dynamics of the system for  $\theta_{\text{fin}} = \pi/2.5$  (larger wetting angle, Fig. 1(d) and Movie 1 in ESI<sup>†</sup>) and  $\theta_{\text{fin}} = \pi/5$  (smaller wetting angle, Fig. 2(b) and Movie 2 in ESI<sup>†</sup>). First, we observe significantly larger distortions of the interface for the system with larger  $\theta_{\text{fin}}$  (compare Movie 1 and Movie 2<sup>†</sup>); as we show below, these

interfacial distortions play an important role in the delivery of the nanoparticles into the lower stream.

Second, the fluid–fluid interface characterized by the larger  $\theta_{\text{fin}}$  displays less curvature; as a result, more of the fin sites are surrounded by the upper fluid for the system with the larger  $\theta_{\text{fin}}$  and hence, more sticky sites have access to adhesive particles in this case than in the scenario with the lower value of  $\theta_{\text{fin}}$ . Independent simulations show that, when the fins remain upright in the binary mixture in the absence of flow (the imposed pressure gradient is 0), the number of adhesive particles attached to the fins saturates at 50 for  $\theta_{\text{fin}} = \pi/2.5$  and saturates at 26 for  $\theta_{\text{fin}} = \pi/5$ . Considering that the imposed flow moves from left to right in the channel, one would expect that sites on the left side of fins can more easily catch particles than sites on the right; this feature reduces the number of accessible sticky sites on the fins to the half of the saturation values in the absence of flow. Thus, a rough estimate of the upper limit of the number of fin–particle bonds formed in the system for  $\theta_{\text{fin}} = \pi/2.5$  is 25 and for the system with  $\theta_{\text{fin}} = \pi/5$  is equal to 13. To test these conjectures, we perform simulations at the following three values of the contact angle:  $\theta_{\text{fin}} = \pi/2.5$ ,  $\pi/5$  and  $\pi/10$ . Here, the remainder of the parameters are held fixed at the reference values.

To quantify the property of catching and releasing nanoparticles into the lower stream, we introduce  $C_a(t)$  and  $C_n(t)$ , which are defined as the number of adhesive and non-adhesive particles in the lower stream relative to the total number of adhesive and non-adhesive particles in the system at time  $t$ , respectively.

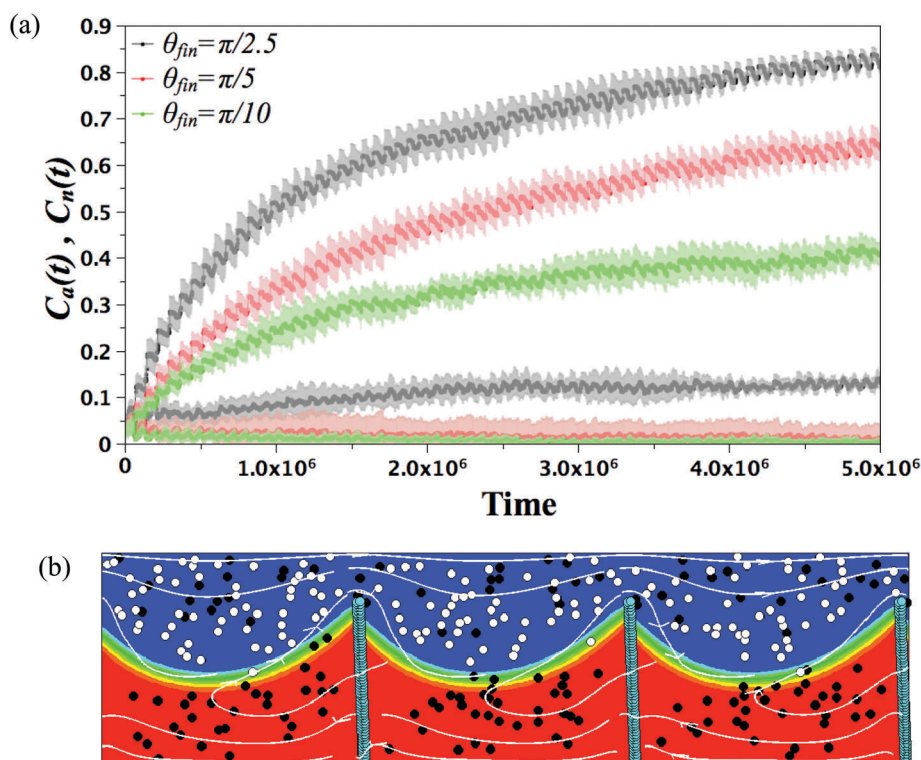


Fig. 2 (a) Temporal evolution of  $C_a(t)$  and  $C_n(t)$  for  $\theta_{\text{fin}} = \pi/2.5$  (black),  $\pi/5$  (red) and  $\pi/10$  (green) with  $N_a = N_n = 150$ . For the curves of the same color, the top and bottom curves correspond to  $C_a(t)$  and  $C_n(t)$ , respectively. (b) Late-time morphology of the system ( $t = 5 \times 10^6$ ) corresponding to the wetting angle  $\theta_{\text{fin}} = \pi/5$ .

$C_a(t)$  characterizes the efficiency of delivering targeted particulates into the lower stream;  $C_a(t) = 1(0)$  corresponds respectively to all (none) of the adhesive nanoparticles being released into the lower stream.  $C_n(t)$  characterizes the accuracy of the delivery process, with  $C_n(t) = 0(1)$  indicating that none (all) of the non-adhesive nanoparticles were unintentionally released into the lower stream.

The top three curves in Fig. 2(a) display the temporal evolution of  $C_a(t)$  for the three different wetting angles:  $\theta_{\text{fin}} = \pi/2.5$  (black),  $\pi/5$  (red), and  $\pi/10$  (green). The solid curves represent the average values over eight independent simulations, and the gray shading indicates the corresponding standard deviations. The curves display small-amplitude oscillations that are comparable for all  $C_a(t)$  and  $C_n(t)$ ; the period of these oscillations is equal to the fins' oscillation period. As discussed for process (2), nanoparticles around the fins will follow the streamlines induced mainly by the fins' oscillations. If those particles are close to the interface (width  $\xi \approx 5$ ) as the fins oscillate between upper and lower phase; this behavior causes the undulation of  $C_a(t)$  and  $C_n(t)$ .

The value of  $C_a(t)$ , however, consistently increases in all three cases, indicating that the number of adhesive particle brought down into the lower phase during the forward stroke always exceeds the number of the particles that are able to escape from this lower phase during the recovery stroke. Ultimately, the values of  $C_a(t)$  approach saturation and larger wetting angles lead to a greater value of  $C_a(t)$ ; *importantly, this indicates that the adhesive particles are delivered into the lower stream with greater efficiency at larger  $\theta_{\text{fin}}$ .*

The latter observations are consistent with the late-time images of the system for  $\theta_{\text{fin}} = \pi/2.5$  (Fig. 1(d)) and  $\theta_{\text{fin}} = \pi/5$  (Fig. 2(b)). A comparison of these late-time snapshots also reveals the other pronounced difference between the two systems: there are no non-adhesive particles within the lower stream for  $\theta_{\text{fin}} = \pi/5$  at  $t = 5 \times 10^6$ , while a small portion of non-adhesive particles are found for  $\theta_{\text{fin}} = \pi/2.5$  at that same time. This difference is reflected in the values of  $C_n(t)$  for these two cases (Fig. 2(a)). For larger wetting angles,  $C_n(t)$  increases and reaches a saturation value around 0.1, which is ten times higher than the value of  $C_n(t)$  for  $\theta_{\text{fin}} = \pi/5$ . Hence, these findings lead

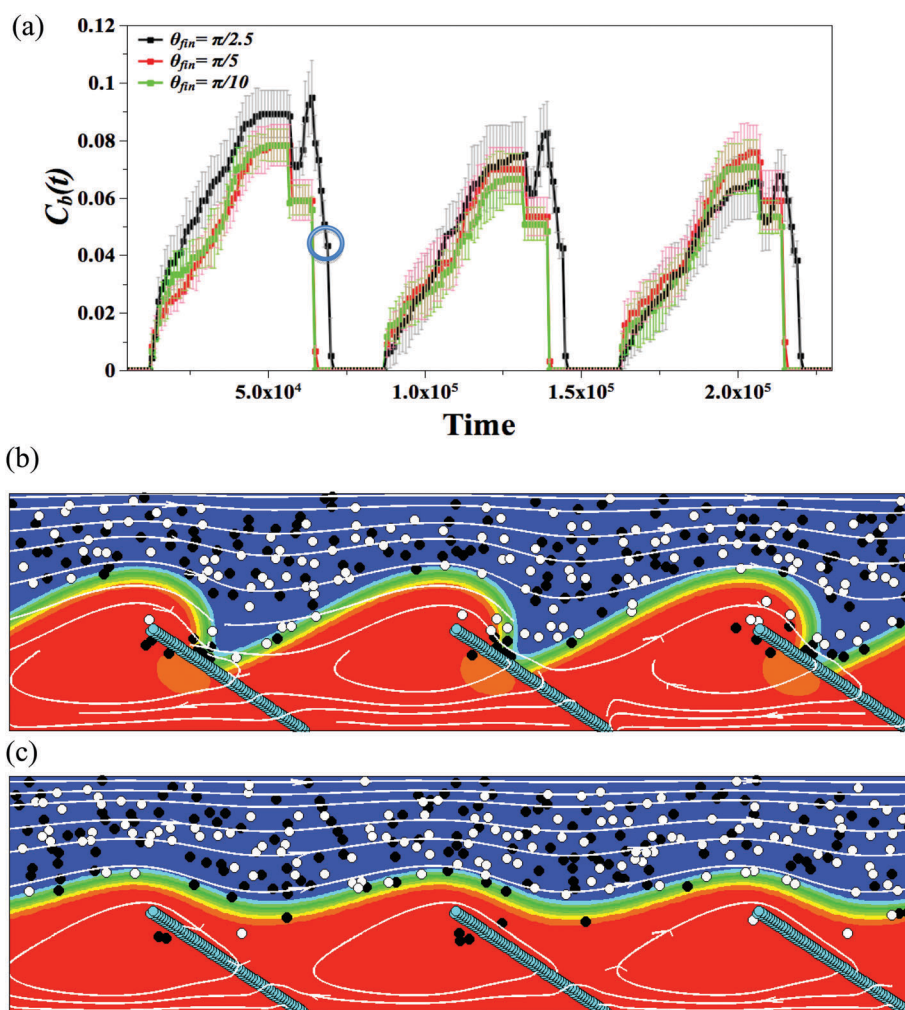


Fig. 3 (a) Temporal evolution of  $C_b(t)$  for wetting angles  $\theta_{\text{fin}} = \pi/2.5$  (black),  $\pi/5$  (red) and  $\pi/10$  (green). (b) Morphology of the system for  $\theta_{\text{fin}} = \pi/2.5$  corresponding to the time frame circled in (a). (c) Morphology of the system for  $\theta_{\text{fin}} = \pi/5$  corresponding to the same time frame as in (b).

to the important conclusion that *at the largest wetting angle considered here, one gains greater efficiency (larger  $C_a(t)$ ) but loses selectivity (larger  $C_n(t)$ ) in the release of the nanoparticles into the lower stream.*

To further characterize these different cases, we introduce the parameter  $\beta$ , which is the ratio of the number of non-adhesive particles to the number of adhesive particles within the lower stream. In our study, the total number of non-adhesive and adhesive particles is set to be equal:  $N_a = N_n$ , and hence,  $\beta = C_n/C_a$ . Thus,  $\beta$  measures the selectivity of the process. The process is nonselective when  $\beta = 1$  since the lower stream contains the same number of adhesive and non-adhesive particles and is the most selective for adhesive particles when  $\beta = 0$ . We find that  $\beta = 0.16, 0.018$ , and  $0.021$  for  $\theta_{\text{fin}} = \pi/2.5, \pi/5$ , and  $\pi/10$ , respectively. Notably, these values indicate that *one can obtain relatively high efficiency without sacrificing the selectivity of the delivery process at the optimal wetting angle  $\theta_{\text{fin}} = \pi/5$ .*

To understand why the “catch and release” process depends on the wetting angle, we monitor the temporal evolution of the fraction of bonds  $C_b(t)$ , defined as the ratio of bonds formed in the system to the total number of adhesive particles. Recall that an adhesive nanoparticle only forms a single bond with an adhesive site on the fin. Fig. 3(a) shows the magnitude of  $C_b(t)$  for three contiguous oscillation cycles. The value of  $C_b(t)$  is indistinguishable among the three wetting angles considered here; hence, the fins catch a similar fraction (peak value  $\approx 7\%$ ) of adhesive particles in all three cases. Note that even though the fins with the larger wetting angles have more accessible sticky sites (25 for  $\theta_{\text{fin}} = \pi/2.5$  and 13 for  $\theta_{\text{fin}} = \pi/5$ ), the number of bonds formed for  $N_a = 150$  is about  $150 \times 7\% \approx 11$ , which is less than the accessible sites on the fin.

A significant difference among the three cases is observed only after  $C_b(t)$  reaches the maximum value and begins to decrease; this decrease corresponds to the fins moving downwards to the lower stream. For example, at the time circled in

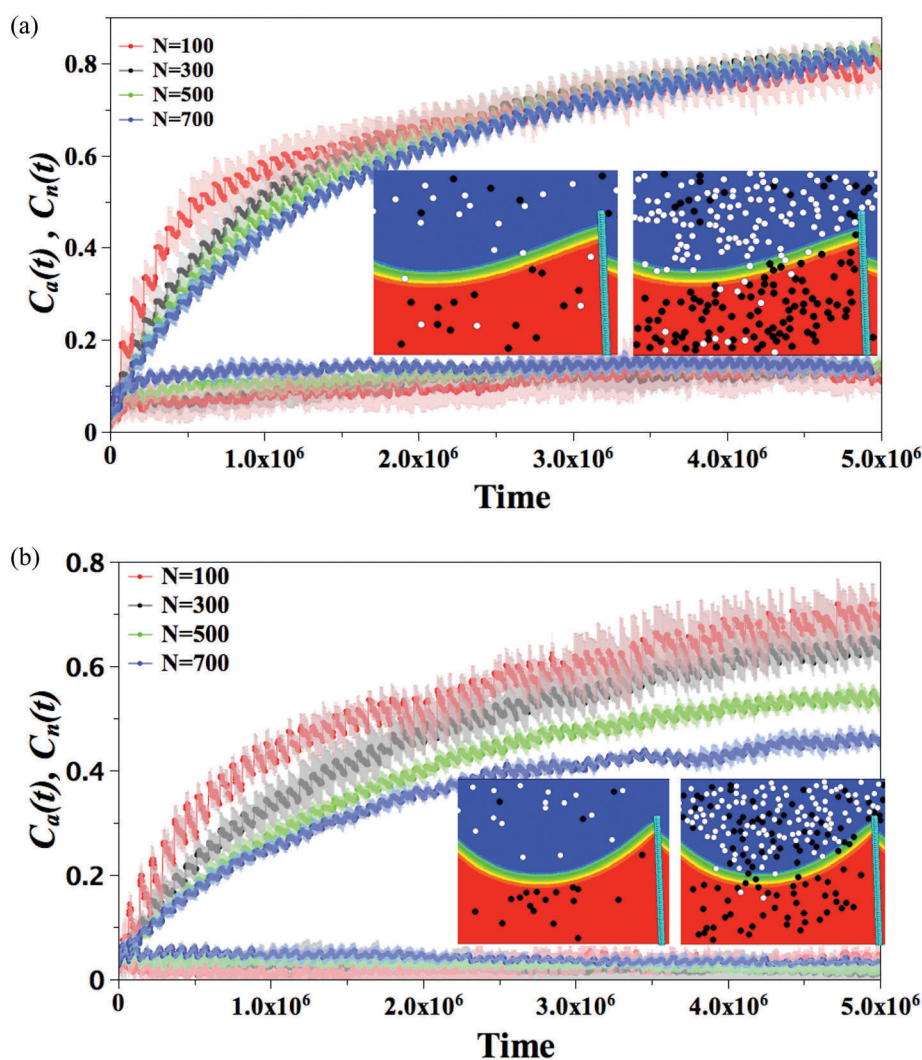


Fig. 4 Time evolution of  $C_a(t)$  and  $C_n(t)$  for different total number of particles  $N$ : 100 (red), 300 (black), 500 (green), and 700 (blue) with the wetting angle: (a)  $\theta_{\text{fin}} = \pi/2.5$  and (b)  $\theta_{\text{fin}} = \pi/5$ . In each figure, top and lower four curves correspond to  $C_a(t)$  and  $C_n(t)$ , respectively. Insets show the late-time ( $t = 5 \times 10^6$ ) morphology of the system for  $N = 100$  (left) and  $N = 700$  (right).

Fig. 3(a),  $C_b(t) \approx 0.043$  for  $\theta_{\text{fin}} = \pi/2.5$ , but is equal to  $C_b(t) = 0$  for both  $\theta_{\text{fin}} = \pi/5$  and  $\pi/10$ . The morphologies corresponding to that moment of time are shown in Fig. 3(b) for  $\theta_{\text{fin}} = \pi/2.5$  and in Fig. 3(c) for  $\theta_{\text{fin}} = \pi/5$ . For the larger wetting angle ( $\theta_{\text{fin}} = \pi/2.5$ ), the interface remains more deformed, especially during the recovery stroke, and the bonds formed between the adhesive particles and these fins can survive for a longer time. Consequently, the adhesive particles are caught and released at a deeper position inside the channel (through process (1)).

Moreover, the fluid convection (indicated by the white streamlines in Fig. 3(b) and (c)) tends to keep the particles localized at these lower positions in the bottom stream. Notably, both of these effects lead to a larger  $C_a(t)$  and higher efficiency of the targeted delivery.

On the other hand, in the case of the smaller wetting angles, the interface undergoes a smaller deformation (Fig. 3(c)). As a result, non-adhesive particles driven into the lower stream are mainly localized near the interface. Due to process (2), these

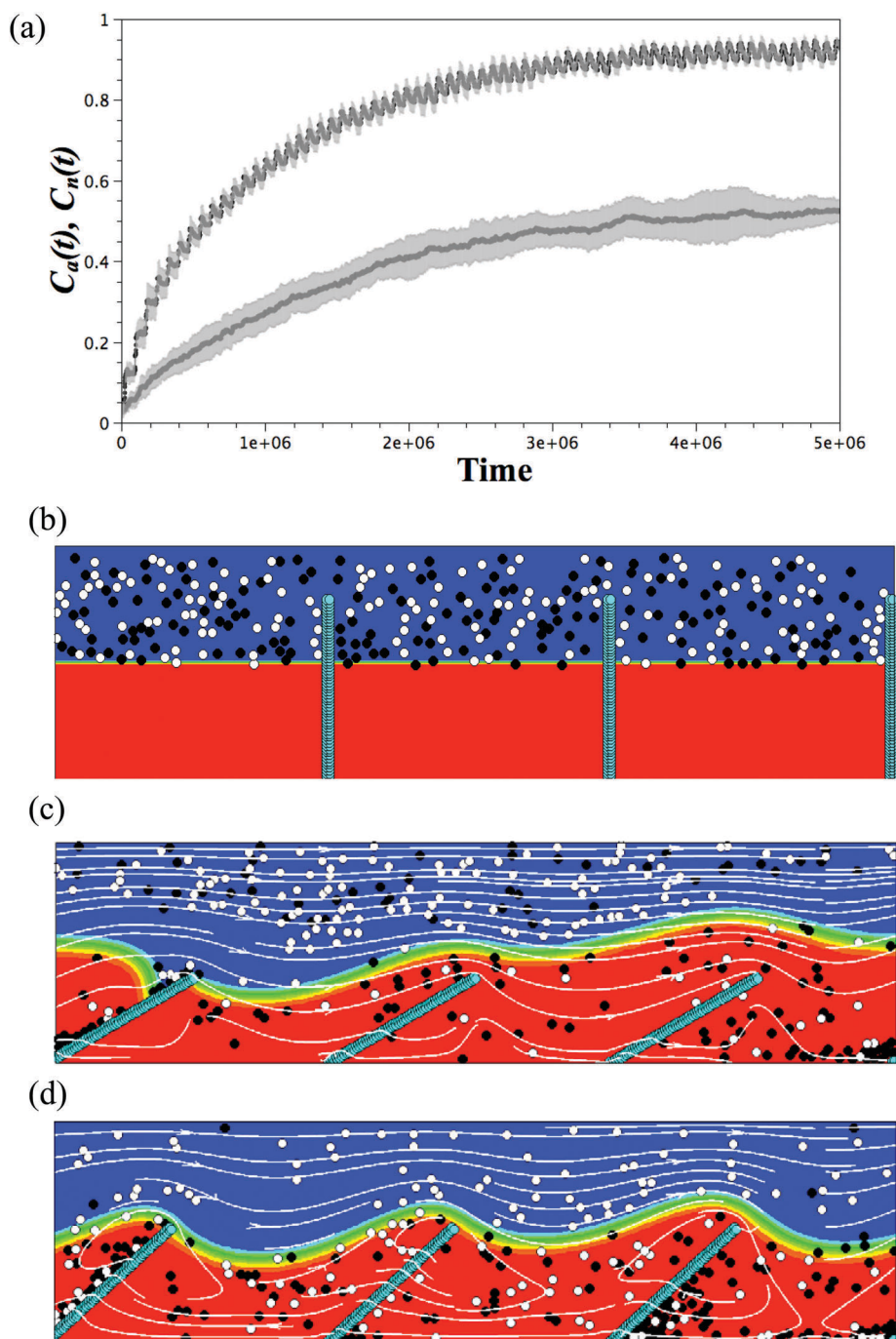


Fig. 5 (a) Temporal evolution of  $C_a(t)$  and  $C_n(t)$  for fins oscillating from  $\pi/2$  to  $5\pi/6$ . (b) Snapshot for initial condition. (c) Morphology of the system when  $\theta = 5\pi/6$  at  $t = 9.3 \times 10^5$ . (d) Late-time morphology of the system at  $t = 5 \times 10^6$ .

non-adhesive particles tend to move back to the upper stream as the fins go up, leading to smaller  $C_n(t)$  and hence, the system exhibits greater selectivity in the delivery of the targeted particles to the lower stream. *Importantly, it is for these reasons that the intermediate value of the contact angle,  $\theta_{\text{fin}} = \pi/5$ , offers the optimal combination of efficiency and selectivity.*

Due to both processes (1) and (2), the number density of particles within the binary mixture will also affect the catch and release of the targeted nanoparticles. To quantify this observation, we analyze the effect of varying the total number of particles, setting  $N = 100, 300, 500$ , and  $700$ . Again, half of the particles are adhesive and half are non-adhesive. Fig. 4(a) and (b) show the temporal evolution of  $C_a(t)$  and  $C_n(t)$  for these different values of  $N$  at  $\theta_{\text{fin}} = \pi/2.5$  and  $\theta_{\text{fin}} = \pi/5$ , respectively. Interestingly, for  $\theta_{\text{fin}} = \pi/2.5$ ,  $C_a(t)$  and  $C_n(t)$  display similar behavior and are relatively insensitive to  $N$ . Note, however, that  $C_a(t)$  increases relatively rapidly at early times for  $N = 100$ . Moreover, snapshots of the system at late times for  $N = 100$  (left inset) and  $N = 700$  (right inset) are significantly different, as shown in Fig. 4(a).

Focusing on the systems with  $\theta_{\text{fin}} = \pi/2.5$ , we monitor the time evolution of  $C_b(t)$  and find that for all the different  $N$ , the plots of  $C_b(t)$  display similar peaks around 7%, indicating that the fins catch similar fractions of adhesive particles in one oscillating cycle. For  $N = 700$ , the number of bonds formed in the system ( $350 \times 7\% \approx 25$ ) is approximately the saturation value for  $\theta_{\text{fin}} = \pi/2.5$ . We can estimate the peak value of  $C_b(t)$  as the ratio of the number of adhesive particles within the regime swept up by the fins in the upper stream to the total number of adhesive particles. Here, we assume the interface between A/B phases remains flat and obtain  $C_b(t) \approx 8\%$ . This value is independent of and is consistent with the simulation results of 7%. Moreover, the number of particles has negligible effects on the streamline profiles since the particles are essentially tracer particulates. Consequently,  $C_a(t)$  and  $C_n(t)$  are independent of the number of particles for the larger wetting angle  $\theta_{\text{fin}} = \pi/2.5$ .

For the smaller wetting angle  $\theta_{\text{fin}} = \pi/5$ , all the plots of  $C_n(t)$  for different  $N$  fluctuate around values close to zero, as anticipated due to the higher selectivity of the delivery process for lower wetting angles. The values of  $C_a(t)$  are, however, smaller for larger number of particles than in the case of  $\theta_{\text{fin}} = \pi/2.5$ . Recall that for  $\theta_{\text{fin}} = \pi/5$ , the saturation value for the number of bonds formed in the system is 13. For  $N \leq 300$ ,  $N_a \times 7\% < 13$ , and hence, the fraction of bonds  $C_b(t)$  can reach the value of 7%; thus, the behavior for  $N = 100$  and  $300$  is indistinguishable. If, however,  $N \geq 500$ , due to the saturation of bonds,  $C_b(t)$  attains smaller values:  $C_b(t) \approx 13/250 \approx 5.2\%$  ( $N = 500$ ) and  $C_b(t) \approx 13/250 \approx 3.7\%$  ( $N = 700$ ), which leads to the smaller value of  $C_a(t)$ . *Notably, it is for this reason that the system at the lower wetting angle shows a dependence on  $N$ .*

The effectiveness of the “catch and release” process can also be tuned by altering the oscillatory behavior of the fins. In the studies described above, the fins moved against the direction of flow and oscillated between the angles  $\theta_{\text{min}} = \pi/6$  and  $\theta_{\text{max}} = \pi/2$ . As before, the fins are initially set upright ( $\theta_{\text{min}} = \pi/2$ ), as shown in Fig. 5(b). Now, however, the fins move along with the direction of flow to  $\theta_{\text{max}} = 5\pi/6$  (Fig. 5(c)), and oscillate between

$\theta_{\text{min}} = \pi/2$  and  $\theta_{\text{max}}$ . Here, we fix  $N = 300$ ,  $T = 1.5 \times 10^5$  and  $\theta_{\text{fin}} = \pi/2.5$ . As shown in Fig. 5(a), both  $C_a(t)$  and  $C_n(t)$  increase to larger values than the scenario with  $\theta_{\text{min}} = \pi/6$  and  $\theta_{\text{max}} = \pi/2$ , (see Fig. 2(a)), with  $C_a(t)$  approaching 90%. The selectivity for the case in Fig. 5 is  $\beta \approx 0.56$ , indicating that a large fraction of both types of nanoparticles are delivered into the lower stream. This observation is also evident from the snapshot of the system at late times displayed in Fig. 5(d). Note that the velocity of the fluid ( $\nu_{\text{fluid}} \approx 2.4 \times 10^{-2} \text{ m s}^{-1}$ ) is much faster than the motion of fins, which can be estimated by the maximal velocity at the tip of fins using eqn (9) and is found to be  $\nu_{\text{fin}} \approx 0.8 \text{ mm s}^{-1}$ . Therefore, when the fins are initially upright, they block the motion of both types of particles, so that the particles clump on the left side of fins since the imposed flow moves from left to right, as shown in Fig. 5(c). When the fins move downwards, those particles are released into the lower stream (Fig. 5(d)), which leads to poor selectivity.

## IV. Conclusions

In summary, we used computational modeling to design an integrated, multi-component system where actuated, microscopic fins controllably catch targeted nanoparticles from the upper fluid stream, transport these particles across a fluid–fluid interface, and then release these particles into the second, lower fluid stream. The particles sequestered in the lower stream can be collected and subsequently removed from the system. By performing this task for multiple cycles, the fins can effectively extract the target particles from the solution. Here, we focused on 50/50 mixtures of targeted and non-targeted particles. The model can also be applied to mixtures containing a lower fraction of targeted particles. With fewer targets in the upper solution, the probability of fin–target interactions becomes smaller, and hence, it will take longer (*i.e.*, more oscillations of the fins) to achieve an effective segregation of the targeted nanoparticles into the lower phase. Notably, if the target nanoparticles were to differ in size, we anticipate that the smaller particles would be extracted first since they display a higher diffusion coefficient and experience less of a frictional drag from the fluid. Hence, there would be a higher probability of collisions between the smaller nanoparticles and the fins than in the case of the more slowly moving larger nanoparticles.

The use of two fluids in this set-up provides a particularly effective means of controlling the binding interactions between the fins and the nanoparticles. For example, as noted in the introduction, the fins can be coated with aptamer that exhibit a binding affinity for the targeted species in the upper fluid, but lose this affinity in the lower stream, and in this manner, the particles can be released from the fins.<sup>3,14</sup> Furthermore, with two immiscible fluids, the wetting interactions (contact angle) between the fins and fluid–fluid (A/B) interface can play an important role in the performance of the system. We did in fact find that by tuning the wetting properties of the microfins, one can enhance the efficiency of separating the target species from the particle mixture, while maintaining a relatively high

selectivity; namely, one can achieve an optimal combination in the efficiency and selectivity of the catch and release behavior. The performance of the device was also found to depend on the fins' mode of oscillation. Specifically, the selectivity of the process was higher in the case where the fins were driven to move against the flow direction from their initial upright location.

The modularity of the system considered here offers distinct advantages for performing *in situ* catch and release processes. The fins can be functionalized with various molecules that display specific binding affinities to particular targeted species, allowing a broad range of compounds to be trapped and extracted.<sup>14,33,34</sup> The binary fluids can also be tailored to promote the binding of the targets in the upper fluid and prompt their release in the lower fluid.<sup>17</sup> The underlying gel, which was assumed to drive the motion of the fins, can be responsive to different environmental cues (*e.g.*, light or heat)<sup>35</sup> and thus, a number of stimuli can be used to drive the oscillations of the fins. Alternatively, the fins could be driven by an imposed oscillating magnetic field.<sup>15–17</sup> Notably, the simulation approach presented here can provide valuable guidelines for fine-tuning the performance of these systems.

## Acknowledgements

The authors gratefully acknowledge financial support from the DOE through grant number DE-SC0005247.

## References

- 1 E. L. V. Harris and S. Angal, *Protein Purification Methods: A Practical Approach*, Oxford University Press, London, 2001.
- 2 J. Arnau, C. Lauritzen, G. E. Petersen and J. Pedersen, *Protein Expr. Purif.*, 2006, **48**, 1.
- 3 J. Fu, P. Mao and J. Han, *Trends Biotechnol.*, 2008, **26**, 311.
- 4 Y. A. Song, S. Hsu, A. L. Stevens and J. Han, *Anal. Chem.*, 2006, **78**, 3528.
- 5 M. Eigen and R. Rigler, *Proc. Natl. Acad. Sci. U. S. A.*, 1994, **91**, 5740.
- 6 E. J. Cho, J. R. Collett, A. E. Szafranska and A. D. Ellington, *Anal. Chim. Acta*, 2006, **564**, 82.
- 7 M. Cabodi, Y. F. Chen, S. W. Turner, H. G. Craighead and R. H. Austin, *Electrophoresis*, 2002, **23**, 3496.
- 8 Z. Zhang, N. Chen, S. Li, M. R. Battig and Y. Wang, *J. Am. Chem. Soc.*, 2012, **134**, 15716.
- 9 T. Arakawa, Y. Shirasaki, T. Aoki, T. Funatsu and S. Shoji, *Sens. Actuators, A*, 2007, **135**, 99.
- 10 L. Chen, X. Liu, B. Su, J. Li, L. Jiang, D. Han and S. Wang, *Adv. Mater.*, 2011, **23**, 4376.
- 11 K. Yoshimatsu, B. K. Lesel, Y. Yonamine, J. M. Beierle, Y. Hoshino and K. J. Shea, *Angew. Chem., Int. Ed.*, 2012, **51**, 2405.
- 12 L. Zhang, A. Chatterjee and K. T. Leung, *J. Phys. Chem. Lett.*, 2010, **1**, 3385.
- 13 X. He, M. Aizenberg, O. Kuksenok, L. D. Zarzar, A. Shastri, A. C. Balazs and J. Aizenberg, *Nature*, 2012, **487**, 214.
- 14 A. Shastri, L. M. McGregor, Y. Liu, V. Harris, H. Nan, M. Mujica, Y. Vasquez, A. Bhattacharya, Y. Ma, M. Aizenberg, O. Kuksenok, A. C. Balazs, J. Aizenberg and X. He, *Nat. Chem.*, 2015, **7**, 447.
- 15 M. Vilfan, A. Potocnik, B. Kavcic, N. Osterman, I. Poberaj, A. Vilfan and D. Babic, *Proc. Natl. Acad. Sci. U. S. A.*, 2010, **107**, 1844.
- 16 J. Toonder, F. Bos, D. Broer, L. Filippini, M. Gillies, J. de Goede, T. Mol, M. Reijme, W. Talen, H. Wilderbeek, V. Khataavkar and P. Anderson, *Lab Chip*, 2008, **8**, 533.
- 17 B. A. Evans, A. R. Shields, R. L. Carroll, S. Washburn, M. R. Falvo and R. Superfine, *Nano Lett.*, 2007, **7**, 1428.
- 18 L. W. Dick, Jr. and L. B. McGown, *Anal. Chem.*, 2004, **76**, 3037.
- 19 A. J. Bray, *Adv. Phys.*, 2002, **51**, 481.
- 20 R. Verberg, J. M. Yeomans and A. C. Balazs, *J. Chem. Phys.*, 2005, **123**, 224706.
- 21 A. J. Briant, P. Papatzacos and J. M. Yeomans, *Philos. Trans. R. Soc., A*, 2002, **360**, 485.
- 22 A. Briant and J. Yeomans, *Phys. Rev. E: Stat., Nonlinear, Soft Matter Phys.*, 2004, **69**, 031603.
- 23 P. de Gennes, *Rev. Mod. Phys.*, 1985, **57**, 827.
- 24 A. Alexeev, R. Verberg and A. C. Balazs, *Macromolecules*, 2005, **38**, 10244.
- 25 A. Bhattacharya and A. C. Balazs, *Soft Matter*, 2013, **9**, 3945.
- 26 S. Succi, *The Lattice Boltzmann equation: for fluid dynamics and beyond*, Oxford University Press, London, 2001.
- 27 M. Swift, E. Orlandini, W. Osborn and J. Yeomans, *Phys. Rev. E: Stat., Nonlinear, Soft Matter Phys.*, 1996, **54**, 5041.
- 28 M. H. Bouzidi, M. Firdaouss and P. Lallemand, *Phys. Fluids*, 2001, **13**, 3452.
- 29 M. E. Cates, K. Stratford, R. Adhikari, P. Stansell, J. C. Desplat, I. Pagonabarraga and A. J. Wagner, *J. Phys.: Condens. Matter*, 2004, **16**, S3903.
- 30 N. Q. Nguyen and A. Ladd, *Phys. Rev. E: Stat., Nonlinear, Soft Matter Phys.*, 2002, **66**, 046708.
- 31 V. M. Kendon, M. E. Cates, I. Pagonabarraga, J. C. Desplat and P. Bladon, *J. Fluid Mech.*, 2001, **440**, 147.
- 32 E. Kim, K. Stratford, R. Adhikari and M. E. Cates, *Langmuir*, 2008, **24**, 6549.
- 33 E. J. Cho, J. W. Lee and A. D. Ellington, *Annu. Rev. Anal. Chem.*, 2009, **2**, 241.
- 34 R. K. Mosing and M. T. Bowser, *J. Sep. Sci.*, 2007, **30**, 1420.
- 35 M. A. Stuart, W. T. Huck, J. Genzer, M. Muller, C. Ober, M. Stamm, G. B. Sukhorukov, I. Szleifer, V. V. Tsukruk, M. Urban, F. Winnik, S. Zauscher, I. Luzinov and S. Minko, *Nat. Mater.*, 2010, **9**, 101.